Spatial and Spatiotemporal Autocorrelation Analysis of Citrus Canker Epidemics in Citrus Nurseries and Groves in Argentina

T. R. Gottwald, K. M. Reynolds, C. L. Campbell, and L. W. Timmer

Respectively, research plant pathologist, USDA, Agricultural Research Service, Horticultural Research Laboratory, Orlando, FL; forest pathologist, USDA, Forest Service, Institute of Northern Forestry, Anchorage, AK; associate professor, North Carolina State University, Raleigh; and professor, University of Florida, Citrus Education and Research Center, Lake Alfred.

Research supported in part by USDA/OICD grant IR-AR-FL-137 and USDA cooperative agreement 58-43 yk-5-3.

We thank L. V. Madden for help and consultation with the STAUTO program and S. Zitko, C. Hurtado, M. Scheifler, V. Scheifler, V. Figueredo, J. Bittle, S. Garran, N. Timmer, and A. Dow for technical assistance.

Accepted for publication 16 April 1992.

ABSTRACT

Gottwald, T. R., Reynolds, K. M., Campbell, C. L., and Timmer, L. W. 1992. Spatial and spatiotemporal autocorrelation analysis of citrus canker in citrus nurseries and groves in Argentina. Phytopathology 82:843-851.

Spatial and spatiotemporal (ST) patterns of citrus canker were examined in three nurseries and two groves in Argentina. The center plant in each plot was inoculated with *Xanthomonas campestris* pv. *citri,* and disease was allowed to progress for two growing seasons. Disease assessments were made at about 21-day intervals. Final disease incidence was >90% in all three nurseries and reached 69 and 89% for orange (*Citrus sinensis*) and grapefruit (*C.* × *paradisi*) groves, respectively. For nursery plots, each quadrat was represented by disease counts, i.e., the number of diseased leaves, in a six-plant row segment. For grove plots, each individual tree was considered a quadrat because of the large number of leaves per tree. Data from each assessment date were analyzed by spatial correlation analysis and by ST autocorrelation analysis. Changes in significantly correlated spatial lags closely followed the changes in the disease progress curves for each plot. Proximity patterns in all three nurseries changed little during the first three to four assessments and then became more complex, often with noncontiguous elements that indicated the formation of secondary foci. Noncontiguous elements remained until the last few assessments, when they eroded and the proximity patterns generally became larger and contiguous as the numerous foci coalesced. Disease incidence increased more rapidly in the grove plots than in the nursery plots. Spatial proximity patterns of disease for the grapefruit grove plot, corresponding to assessment dates immediately after a rainstorm with high winds, were elongated in the north-south direction. In contrast, spatial proximity patterns in the orange grove plot were more radially symmetrical until later in the epidemic, when they became more elongate in the north-south orientation and a few noncontiguous elements developed. ST autocorrelations and partial autocorrelations from the ST autocorrelation analysis of nurseries and groves were generally highest with a square proximity pattern. For citrus nurseries, ST autocorrelations and partial autocorrelations were consistent over time. ST autocorrelations decayed rapidly over spatial lags, but remained significant to four temporal lags. Therefore, the ST transfer function for citrus nurseries infected with citrus canker was represented by a ST autoregressive integrated moving-average (STARIMA) model, STARIMA(0,4,1,1). The ST partial autocorrelations were similar for both grove plots, indicating a similarity in the autoregressive components of each grove and, thus, a STARIMA model structure, but the two groves differed in inclusion of moving-average terms. For the orange grove, autocorrelations for the first temporal lag decayed slowly over the first three spatial lags, whereas the autocorrelation for the first temporal lag in the grapefruit grove decayed rapidly over spatial lags. Also, significant moving-average effects were estimated to extend to two temporal lags in the grapefruit grove data but to only one in the orange grove data. Thus, STARIMA model forms for the orange and grapefruit groves were estimated to be STARIMA(0,1,4,1) and STARIMA(0,2,1,2), respectively.

Citrus canker, caused by *Xanthomonas campestris* pv. *citri,* is characterized by erumpent lesions on fruit, foliage, and young stems of susceptible cultivars of citrus. When disease is severe, defoliation and dieback can occur and infected fruit are less valuable or entirely unmarketable (13,14). In Argentina, citrus canker is an endemic foliar disease introduced in 1976, most likely from Japan (14). Citrus canker in Argentina is normally controllable with a combination of windbreaks to reduce infection by windblown rains and copper-containing bactericidal sprays. The disease can cause nominal to significant damage, however, during seasons when spring and summer rains are combined with wind speeds in excess of 8 m/s (19,21,22). In an attempt to prohibit the introduction of the disease, many citrus-growing areas restrict the importation of citrus from areas or countries known to be infested.

In citrus nurseries infested with citrus canker, dissemination of *X. c. citri* is primarily by splash dispersal (12,23). The result is the development of numerous secondary foci that eventually coalesce in larger, irregularly shaped areas of disease, which makes the description and quantification of disease gradients difficult and of limited value. Slopes of disease gradients associated with citrus canker in nurseries fluctuate over time because of disease-induced defoliation on severely diseased nursery plants and infection of newly emerging foliage (12). Lloyd's index of patchiness (24) has previously been used to demonstrate highly significant aggregation of disease associated with splash dispersal, which decreased as the secondary foci coalesced (12). Ordinary-runs analysis also was used to demonstrate a slightly higher within-nursery than across-nursery row aggregation, although aggregation was demonstrable in all nurseries studied throughout the epidemics, irrespective of direction (12).

In epidemics of citrus canker in citrus groves in Argentina, slopes of disease gradients also fluctuated in response to disease-induced defoliation. However, unlike citrus nurseries, gradient slopes were directly related to windblown rain direction. They were shallowest downwind and steepest upwind from the foci of infection (10). Slopes of disease progress curves calculated with the linear form of the Gompertz model also were significantly greater in the downwind direction. Aggregation of diseased trees was indicated by both ordinary-runs analysis and doublet analysis throughout the epidemics (10).

Several statistical procedures exist for the quantitative analysis of spatial patterns of disease (2,4,16,17,24). Although these procedures are highly useful in describing distribution patterns of disease, all are restricted to analysis at a single point in time. One particularly useful method of describing spatial relationships among diseased areas (quadrats) is the spatial lag autocorrelation (SLA) analysis (2,3,18), which identifies two-dimensional proximity patterns among quadrats and not simply within-row and

across-row associations. SLA has been used to describe the spatial relationships of other citrus diseases, including citrus greening disease in China and citrus bacterial spot epidemics in Florida (7,9). The analysis provides correlation matrices that estimate the spatial relationship of plants or quadrats. For SLA, the subscripts i and j denote the position of quadrats within a rectangular grid, such that $i = 1, 2, \ldots$ and $j = 1, 2, \ldots$ designate row and column numbers, respectively. The correlations at various distances (lags) are then $p(l,k)$ where $l = i'-i$ and $k = j'-j$ define the two-dimensional lags or number of quadrats from quadrat (i,j) across rows and across columns, respectively, to quadrat (i',j') (11). Recent availability of the ST autocorrelation analysis (20) provides the ability to examine the evolution of an epidemic in both space and time simultaneously (1,15,21). The results of ST autocorrelation analysis led to the description of an ST transfer function in the form of a mixed ST autoregressive integrated moving average (STARIMA) model. The STARIMA model takes the form STARIMA(l,m,p,q), in which the autocorrelations begin to decay after p–l lags in space and q–m lags in time and the partial autocorrelations begin to decay after the first l–p lags in space and m–q lags in time (20). STARIMA models summarize the spatial and temporal dependencies in the data and account for the evolution of the observed patterns, providing insight into both the spatial and temporal processes of the dynamics of disease epidemics.

The purpose of this study was to examine the spatial relationships of citrus canker on trees in infested nurseries and groves over time and to relate these relationships to possible biological factors, including the relative susceptibilities of citrus cultivars.

MATERIALS AND METHODS

Plots were established in three citrus nurseries and two citrus groves at the experiment station of the Instituto Nacional de Tecnologia Agropecuaria in Concordia, Entre Rios, Argentina, between 1985 and 1987. The first two nurseries consisted of seedlings of Pineapple sweet orange, *Citrus sinensis* (L.) Osbeck, and Duncan grapefruit, *C.* × *paradisi* Macfady, each planted with 11 rows of 45 seedlings per row, approximately 0.6 m between rows, and 0.15 m between plants within rows. The third nursery consisted of seedlings of Swingle citrumelo, *Poncirus trifoliata* (L.) Raf. × *C.* × *paradisi,* planted in 15 rows of 67 plants per row and with the same spacing as the other nurseries. Both citrus groves were planted with a 5-m spacing between trees in a row and across rows as a grid of 11 × 11 trees of either Duncan grapefruit or Valencia sweet orange. Water was applied to plants by overhead irrigation two to three times per week in the summer when there was no rain. The cultivars ranged in susceptibility to citrus canker as follows: Swingle citrumelo, moderately susceptible; Pineapple sweet orange, moderately to highly susceptible; and Duncan grapefruit, highly susceptible.

The center (focal) plant in each nursery was inoculated with an isolate of *X. c. citri* originally obtained from an infected grapefruit leaf. Plantings were about 6 mo old at the time of inoculation. The isolate was grown on nutrient agar for ~72 h at 27 C. Bacteria were harvested, suspended in 0.07 M phosphate buffer, pH 6.8, and adjusted turbidometrically to ~10^8–10^{10} cfu/ml. All foliage of the designated focal plants (about 100 to 200 leaves) was dusted lightly with Carborundum, thoroughly wetted with the bacterial suspension, and rubbed with bare hands to cause small wounds for infection. Disease developed about 7–10 days after inoculation.

Disease assessments were made every ~21 days during the growing season and every ~30 days during the winter months. Assessments of disease incidence (number of leaves infected/total number of leaves per plant) were made for each plant in each plot for a total of 13, 13, and 23 assessments for the orange, grapefruit, and Swingle citrumelo nursery plots, respectively, and 22 assessments each for the orange and grapefruit grove plots.

To tabulate disease within nursery beds, rows were partitioned into 0.8-m-long segments, each containing six seedlings in quadrats 0.8 m long and 0.6 m wide. This quadrat size allowed a more nearly squared lattice of plants. Disease incidence within a nursery quadrat was expressed as the mean of the incidence of the six seedlings. For groves, individual trees were treated as quadrats and incidence expressed as the total number of diseased leaves per tree.

Rainfall, temperature, and wind speed were measured with a

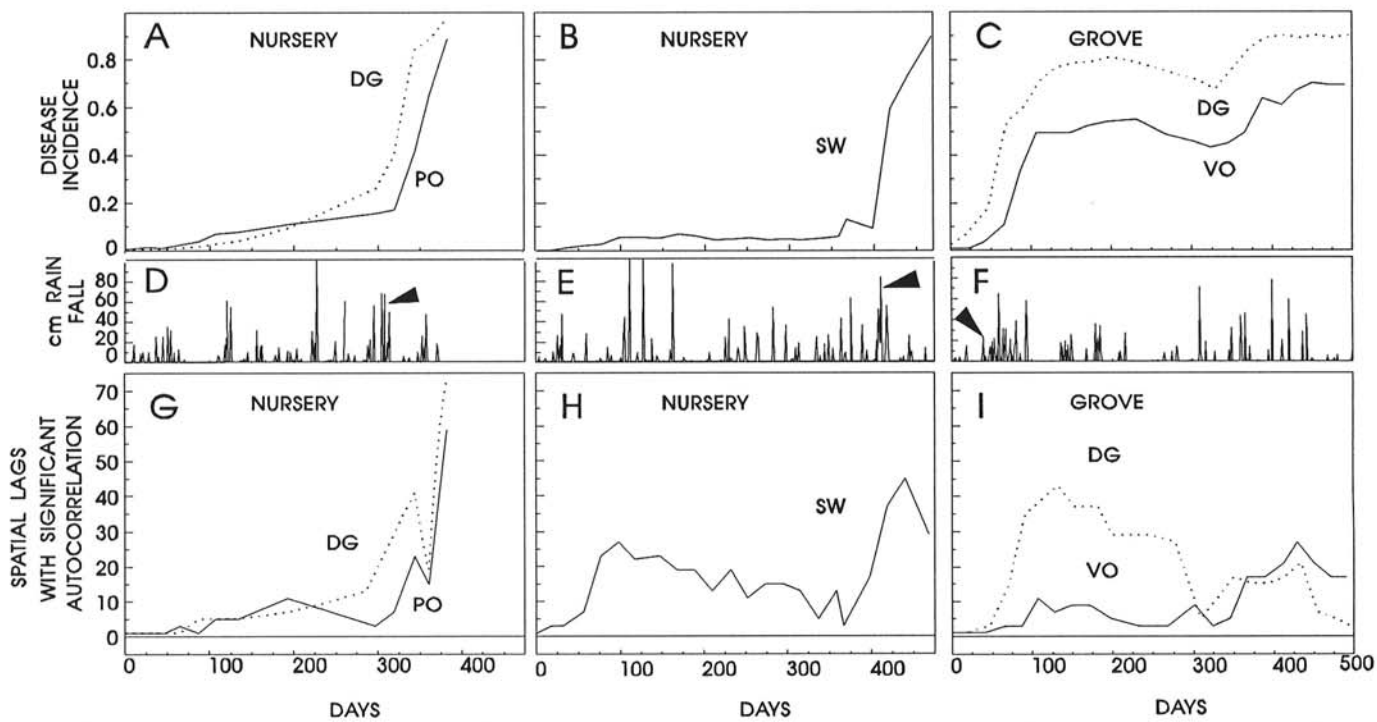

Fig. 1. Disease progress curves for citrus canker in **A,** Duncan grapefruit and Pineapple orange nurseries; **B,** Swingle citrumelo nursery; **C,** Duncan grapefruit and Valencia orange groves. **D–F,** Arrows indicate rainstorms associated with winds >8 m/s. **G–I,** Change in the number of spatial lags with significant autocorrelations over time determined by spatial lag autocorrelation analysis. DG, Duncan grapefruit; PO, Pineapple orange; SW, Swingle citrumelo; VO, Valencia orange.

tipping bucket rain gauge, a thermistor probe, and an anemometer, respectively, connected to a micrologger system (Model 21X, Campbell Scientific, Inc., Logan, UT).

SLA analysis was performed on all nursery and grove data sets for each assessment date to compute the spatial autocorrelation among incidence values in quadrats (3,16,18). The SLA analysis was performed using LCOR2 (8), which computes correlation matrices in which the value of disease incidence in each quadrat is compared with the values in all proximal quadrats. The proximity pattern for each plot by date was estimated by interpreting the correlation matrices (3,20). The individual proximity patterns were represented graphically on a time line using the three-dimensional capabilities of the AUTOCAD program (AUTOCAD386 version 11, Autodesk, Inc., Sausalito, CA). SLA analysis also permits the comparison of correlation matrices derived from diagonal orientations in relationship to the rectangular data matrix (8). Asymmetry or skewness of the proximity pattern can be determined by comparison of the diagonal correlation matrices.

Data for the first three assessment times were deleted from the three nursery data sets before analyses to ensure stationarity of the ST process (20). Data for the first two assessment times

TABLE 1. Spatial lag autocorrelations of incidence of citrus canker for day 392 (assessment 17) in a grapefruit grove plot in Argentina

Lags north-south	Lags east-west								
	0	1	2	3	4	5	6	7	8
0	1.00000	0.27272**[a]	0.18185	0.32263**	0.09368	−0.05384	0.17026	−0.13573	−0.17466
1	0.44145**	0.23437*	0.07786	0.16522	0.00580	−0.04683	0.07677	−0.26090	−0.31945
2	0.32773**	0.03693	−0.08135	0.21132	−0.19430	−0.17453	0.07669	−0.34757	0.50630
3	0.21296*	−0.01546	−0.19090	0.03563	−0.15076	−0.21713	−0.06128	−0.16547	−0.38073
4	0.18870	−0.05784	−0.22516	0.05665	−0.30723	0.27843	0.08324	−0.33678	−0.33092
5	0.03941	−0.19050	−0.19386	−0.14904	−0.29278	−0.24034	−0.00294	−0.28484	−0.20923
6	0.09753	−0.10506	−0.18342	0.00135	−0.26144	−0.25730	0.08222	−0.25179	−0.24294
7	0.02681	−0.08525	−0.16412	−0.07239	−0.20575	−0.16424	−0.14611	−0.20937	−0.48775
8	0.07064	−0.05802	−0.19120	−0.13983	−0.26811	−0.16938	0.03145	−0.54863	−0.23140

[a] Autocorrelations significantly different from zero at $P = 0.05$ and 0.01 for * and **, respectively.

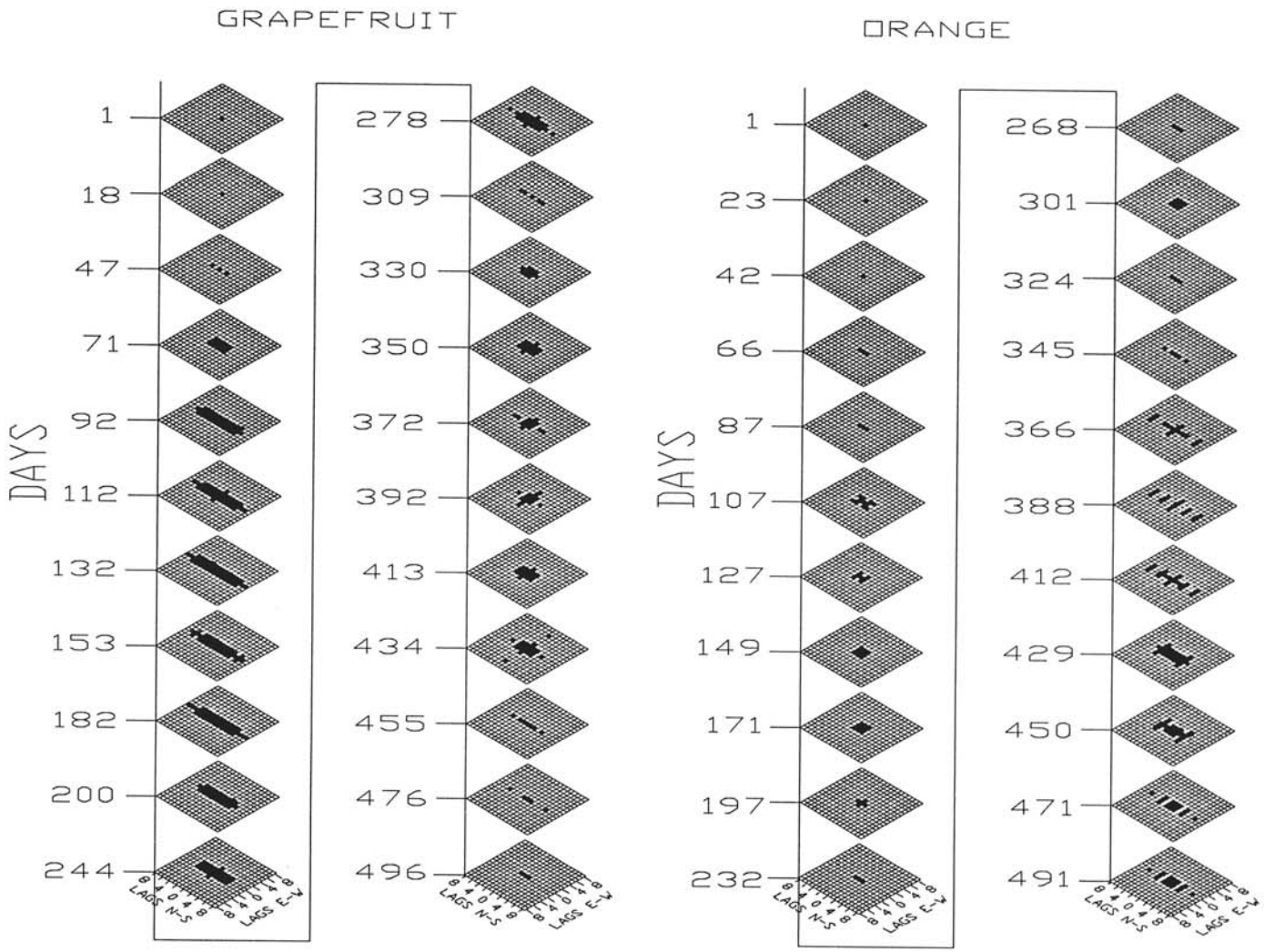

Fig. 2. Proximity patterns for citrus canker determined by spatial lag autocorrelation analysis for two citrus groves in central Argentina. Darkened squares in each grid indicate significant ($P = 0.05$) autocorrelations at that lag in east-west and north-south distances. Proximity patterns are presented on time lines corresponding to assessment dates. Compare assessment dates with disease progress curves in Figure 1A–C.

were deleted from the grove data before analyses for the same reason. For each nursery and grove data set, spatial autocorrelations and spatial partial autocorrelations were computed for each assessment time with the ST autocorrelation program STAUTO (20) by setting the maximum temporal lag order to 0. Binary weighting and the rook proximity pattern were used in the spatial autocorrelation analysis of each data set (20).

In the nurseries and groves, epidemics originated from foci as a result of artificial inoculation, and disease progress curves always exhibited a general trend of linear increase. Therefore, before all ST autocorrelation analyses with STAUTO, values of logit(incidence) were transformed by performing simultaneous spatial and temporal differencing to assure temporal and spatial stationarity (20). The STAUTO program can produce spatial autocorrelation analyses for each assessment time and an ST autocorrelation analysis for all assessment times. ST correlograms and partial correlograms for the rook, queen, and square proximity patterns were compared with one another to select the pattern producing the highest overall level of correlation. Binary weighting was used in all comparisons of proximity patterns. Patterns of ST autocorrelations and partial autocorrelations were evaluated to identify significant moving-average and autoregressive components, respectively, of STARIMA model structure (1,20).

RESULTS

Incidence of citrus canker increased slowly in all three nurseries (Fig. 1). Logarithmic increases in incidence were associated with a series of rainstorms that occurred during the second growing season. In contrast, disease increase in both grove plots followed rainstorms with high winds that occurred soon after the plots were established during the first growing season (Fig. 1). After initial spread of the disease, the weather was often dry, and wet periods were not accompanied by high winds. Therefore, no disease increase occurred, and some defoliation of older leaves led to a slight decline in disease incidence during the winter and following spring. For all plots, summer rains during the second season were again associated with pathogen dispersal and disease development, contributing to disease increase during the second season that leveled off during the dry fall period (Fig. 1). Disease incidence decreased slightly in all five plots during the winter months after the first growing season.

To demonstrate the SLA analysis, an example of a SLA correlogram is given for the grapefruit grove plot on day 392 of the epidemic, which is generally representative of the SLA results observed (Table 1). For the example, there was a significant correlation between incidence in each quadrat and in one and three quadrats in an east-west direction and one, two, and three

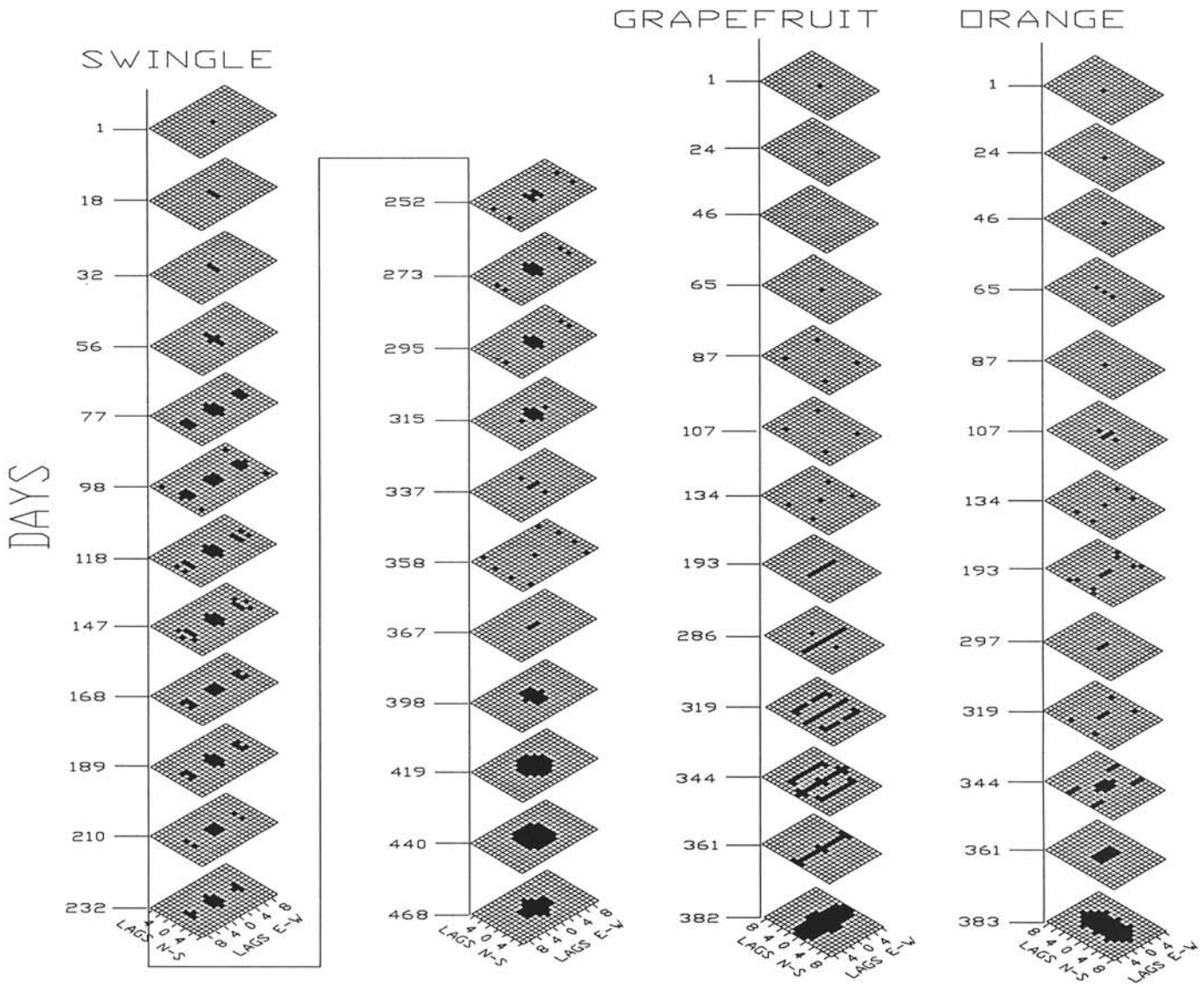

Fig. 3. Proximity patterns for citrus canker determined by spatial lag autocorrelation analysis for three citrus nurseries in central Argentina. Darkened squares in each grid indicate significant ($P = 0.05$) autocorrelations at that lag in east-west and north-south distances. Proximity patterns are presented on time lines corresponding to assessment dates. Compare assessment dates with disease progress curves in Figure 1A–C.

quadrats in the north-south direction. The resulting proximity pattern determined from the interpretation of this correlogram is shown in Figure 2 (grapefruit grove time line, day 392). The number of spatial lags with significant autocorrelations was directly related to disease incidence. Decreasing disease incidence during the winter after the first growing season resulted in a decrease in number of spatial lags with significant autocorrelations for the orange and Swingle citrumelo nurseries, as well as for the grapefruit and orange grove plots.

Proximity patterns in all three nurseries studied changed little if at all during the first three to four assessments of the epidemics (Fig. 3). Following this initial lack of change, proximity patterns of disease incidence in the nurseries rapidly became more complex, often with noncontiguous elements. These noncontiguous elements remained in one form or another until the last few assessments, when they eroded and the proximity patterns generally became large and contiguous.

Proximity patterns associated with the two citrus grove plots had fewer noncontiguous elements (Fig. 2). Disease developed more rapidly in the grove plots than in the nursery plots, in association with a rainstorm with high winds from the southwest early in the epidemic that resulted in pathogen spread and disease development primarily to the north of the focus. Disease proximity patterns for the grapefruit grove plot, corresponding to assessment dates immediately after this spread, were elongated in the north-south direction (Fig. 2). In contrast, spatial proximity patterns in the grove plot of less susceptible sweet orange were more radially symmetrical until later in the epidemic, when they became more elongated in the north-south orientation and developed a few noncontiguous elements (Fig. 2).

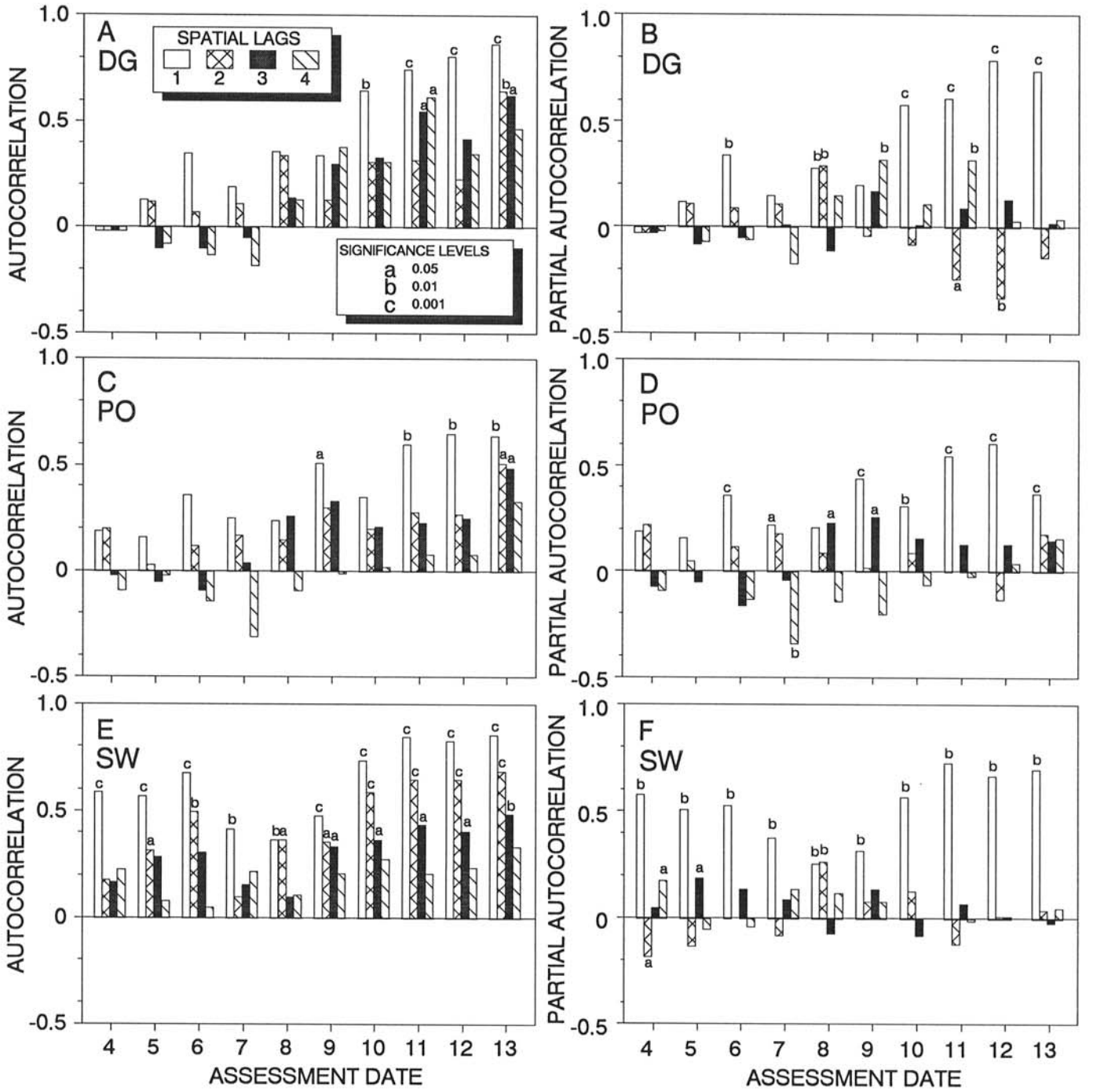

Fig. 4. Spatial autocorrelations and partial autocorrelations for citrus nursery plots infested with citrus canker in Argentina. **A** and **B,** Duncan grapefruit (DG) nursery; **C** and **D,** Pineapple orange (PO) nursery; **E** and **F,** Swingle citrumelo (SW) nursery. Spatiotemporal autocorrelation analyses are based on rook pattern and binary weighting.

Asymmetry or skewness of proximity patterns was only rarely indicated by SLA for any of the data sets and was never temporally stable from one assessment date to another. Therefore, asymmetry where it occurred was considered a minor aberration and ignored.

ST autocorrelation analysis of nursery data. Temporal trends in spatial autocorrelations and partial autocorrelations differed among the three nurseries (Fig. 4). For the Swingle nursery (Fig. 4E and F), autocorrelations were consistently significant at one spatial lag, and, for times 9 (day 232) through 13 (day 315), autocorrelations of up to three spatial lags were significant. This was due to the development of larger aggregates of disease during the later assessment periods. In contrast, for the orange and grapefruit nurseries, autocorrelations at the first spatial lag only became consistently significant by assessment times 11 (day 344) and 10 (day 319), respectively, and significant autocorrelations at higher-order spatial lags did not become significant until times 13 (day 382) and 11 (day 344), respectively. Patterns of spatial partial autocorrelations, which account for the influence of spatial autocorrelations at lower-order spatial lags, were generally similar for the Swingle citrumelo and orange nurseries toward the end of the assessment periods, in that only first-order spatial partial autocorrelations were significant after time 9 (day 168, Swingle, and day 297, orange). This pattern of significance indicated that the occurrence of larger aggregates during this period resulted from coalescence of smaller aggregates, as previously reported (11). At assessment times 11 (day 344) and 12 (day 361), second-order spatial partial autocorrelations were significantly negative for the grapefruit nursery, resulting from disease that occurred in a checkerboard pattern due to intensification of small secondary foci within some quadrats and not others.

In the ST autocorrelation analyses of the nursery data, autocorrelations were generally highest with the square proximity pattern for which ST autocorrelations and partial autocorrelations were never significant beyond one spatial lag. Consequently, alternatives to binary weighting were not considered because they would have had no effect on correlogram structure (20,21). In contrast to the varying trends among the three nurseries in spatial autocorrelations and partial autocorrelations over time (Fig. 4), patterns in ST autocorrelograms and partial autocorrelograms were consistent among nurseries (Fig. 4, Tables 2 and 3). Patterns for the grapefruit nursery were typical; significant ST autocorrelations were absent after one temporal lag and decayed rapidly within the first temporal lag (Fig. 5). ST partial autocorrelations decayed rapidly over spatial lags but remained significant out to four temporal lags. Therefore, all correlogram patterns for the three nurseries were representative of a STARIMA(0,4,1,1) model.

ST autocorrelation analysis of grove data. Temporal trends in spatial autocorrelations and partial autocorrelations also differed between the orange and grapefruit groves (Fig. 6). In the orange grove, aggregations of disease had developed by time 5

TABLE 2. Spatiotemporal autocorrelations with square definition of proximity and binary weighting for logit-transformed incidence of leaves with citrus canker symptoms in an orange nursery plot

Temporal lag order	Spatial lag order 0	1	2	3	4
Spatiotemporal autocorrelation coefficients[a]					
1	−0.2783***	0.2399**	−0.1256	0.0375	0.0288
2	−0.0149	−0.0280	0.0736	−0.0096	0.0321
3	−0.1204	0.0696	−0.0087	0.0276	0.0065
4	−0.0743	0.0674	−0.0471	−0.0125	0.0379
Z-statistics for autocorrelation coefficients					
1	−3.3709	2.9049	−1.5214	0.4542	0.3493
2	−0.1808	−0.3393	0.8916	−1.1604	0.3893
3	−1.4512	0.8391	−0.1053	0.3323	0.0779
4	−0.8935	0.8114	−0.5662	−0.1508	0.4560
Partial autocorrelation coefficients					
1	−0.1821***	0.0122	−0.0176	0.0103	0.0522
2	−0.1371**	−0.0439	−0.0517	−0.0795	0.0055
3	−0.1535***	−0.0365	0.0020	0.0233	0.0574
4	−0.1212**	−0.0370	−0.0433	−0.0251	0.0246

[a] Spatiotemporal autocorrelations were significant at $P = 0.05$, 0.01, and 0.001 for *, **, and ***, respectively. The hypothesized model for the data was STARIMA(0,4,1,1) on the basis of the above.

TABLE 3. Spatiotemporal autocorrelations with square definition of proximity and binary weighting for logit-transformed incidence of leaves with citrus canker symptoms in an Swingle citrumelo nursery plot

Temporal lag order	Spatial lag order 0	1	2	3	4
Spatiotemporal autocorrelation coefficients[a]					
1	−0.3597***	0.2889***	−0.0940	0.0244	−0.0549
2	0.0140	−0.0524	0.0868	−0.0702	0.0191
3	−0.1089*	0.0832	−0.0863	0.0320	0.0608
4	0.0129	−0.0012	−0.0022	0.0178	−0.0261
Z-statistics for autocorrelation coefficients					
1	−5.9649	4.7902	−1.5594	0.4044	−0.9101
2	0.2315	−0.8690	1.4395	−1.1640	0.3172
3	−1.7982	1.3744	−1.4261	0.5292	1.0041
4	0.2127	−0.0199	−0.0360	0.2934	−0.4307
Partial autocorrelation coefficients					
1	−0.2474***	0.0670	0.0130	−0.0313	−0.0539
2	−0.1489***	0.0279	0.0122	−0.0483	−0.0503
3	−0.1732***	−0.0354	−0.0464	−0.0298	0.0217
4	−0.0767*	−0.0049	−0.0191	−0.0125	−0.0056

[a] Spatiotemporal autocorrelations were significant at $P = 0.05$, 0.01, and 0.001 for *, **, and ***, respectively. The hypothesized model for the data was STARIMA(0,4,1,1) on the basis of the above.

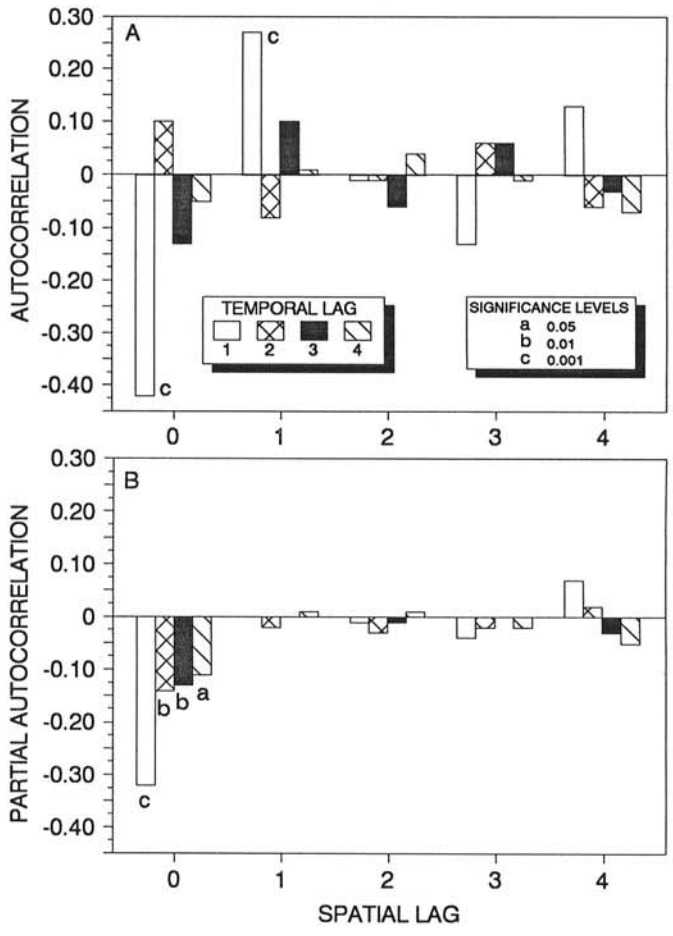

Fig. 5. A, Spatiotemporal autocorrelation, and **B,** partial autocorrelation for a citrus canker-infested grapefruit nursery in Argentina. Analysis was performed with the STAUTO program, with a square-proximity pattern and binary weighting. Logit(incidence) and simultaneous spatial and temporal differencing were used to assure spatial and temporal stationarity.

(day 87), as indicated by the occurrence of significant spatial autocorrelations out to three spatial lags. The patchy pattern of disease in the orange grove persisted through the end of the experiment (Fig. 5). With the exception of assessment time 5, spatial partial autocorrelations did not become significant beyond the first spatial lag until time 17 (day 388) because of aggregations that were composed of smaller, distinctive foci before time 17. Trends in spatial autocorrelations and partial autocorrelations

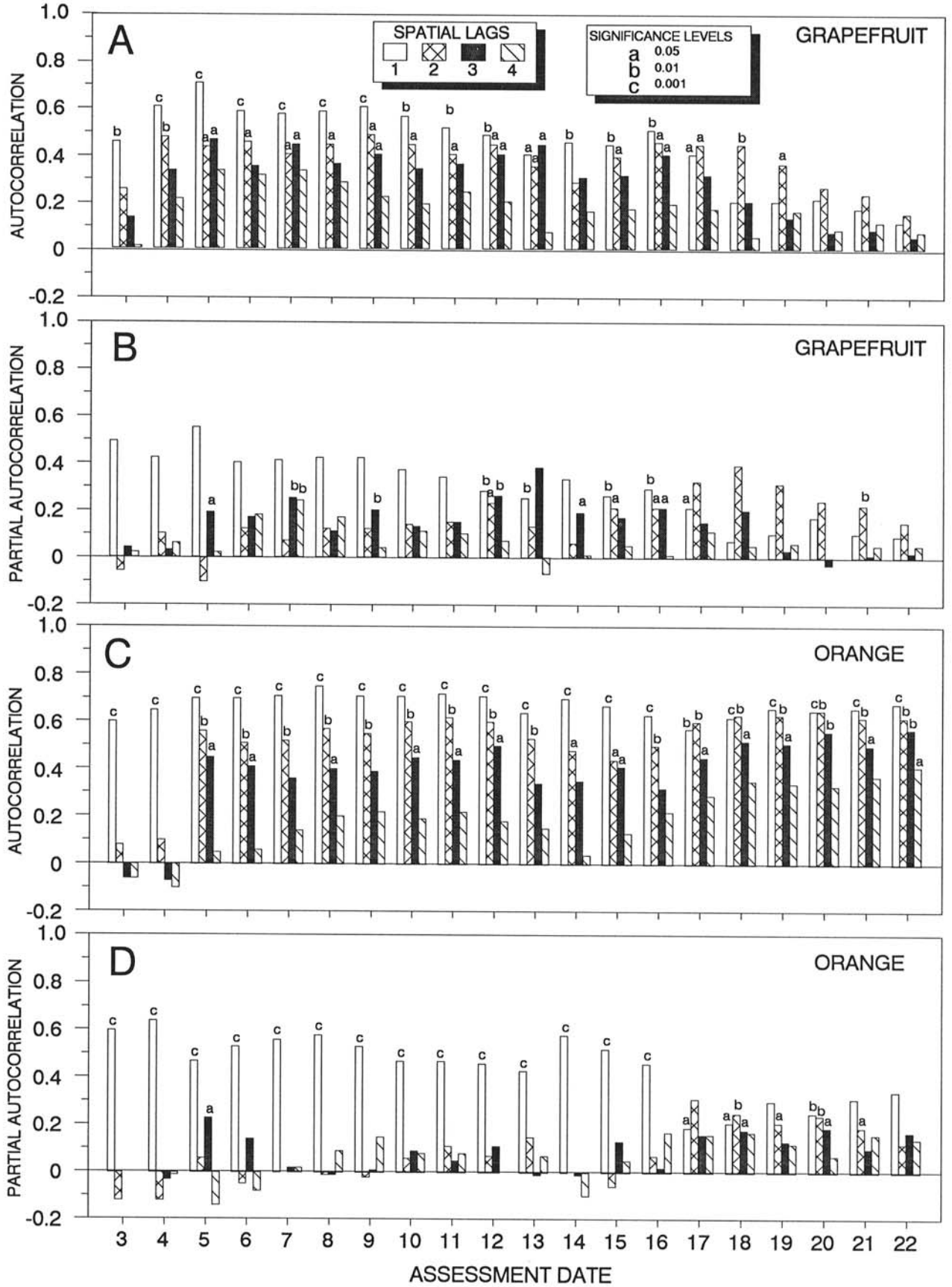

Fig. 6. Spatial autocorrelations and partial autocorrelations for **A** and **B,** grapefruit grove plots, and **C** and **D,** orange grove plots in Argentina infested with citrus canker. Analysis was performed with the STAUTO program, with a rook proximity pattern and binary weighting.

were similar for the grapefruit grove. The most obvious difference between the orange and grapefruit grove patterns was the gradual disappearance of distinct patches in the grapefruit grove beyond time 16 (day 372) (Fig. 6).

As with the ST autocorrelation analysis for nurseries, ST autocorrelations in the grove data were generally highest with the square proximity pattern. Correlograms for the ST partial autocorrelations were similar for the orange and grapefruit groves, indicating a similarity in the autoregressive components of each grove's respective STARIMA model structure (Fig. 7). However, the two groves differed with respect to the inclusion of moving-average terms. In the orange grove data, autocorrelations at the first temporal lag decayed slowly over spatial lags and became nonsignificant only after the third spatial lag (Fig. 7A and B). In contrast, ST autocorrelations at the first temporal lag decayed rapidly in the grapefruit grove data (Fig. 7C and D). Moreover, significant moving-average effects (i.e., significance of the autocorrelation function but not the partial autocorrelation function) extended to two temporal lags in the grapefruit grove data but were cut off after the first temporal lag in the orange grove data. The STARIMA model forms for the orange and grapefruit groves were therefore hypothesized to be STARIMA(0,1,4,1) and STARIMA(0,2,1,2), respectively.

DISCUSSION

In previous studies, rain splash was the dominant factor contributing to disease development and the establishment of secondary foci of citrus canker in citrus nurseries (9,12,23). The combined effects of within-row and between-row spacing of plants in the nursery and the frequency of rains with no wind mask the directional spread of citrus canker due to occasional wind-blown rainstorms (12). In contrast, the greater spacing between grove trees is too far for simple rain splash dispersal. Blowing rainstorms are required for inoculum to be spread from tree to tree (5,9,10,13,23).

SLA analysis. The occurrence of the noncontiguous elements of the citrus nursery proximity patterns coincided with the development of secondary foci from rain splash dispersal of inoculum (Fig. 3). The disappearance of the noncontiguous elements later in the epidemic corresponded to the logarithmic increase phase of the disease progress curves associated with the individual citrus nurseries (Fig. 3). As disease incidence exceeded 0.5 in each nursery, the secondary foci formed by splash dispersal began to coalesce (Fig. 1) (12). Thus, the noncontiguous proximity pattern elements eroded and were replaced by larger contiguous proximity patterns. Furthermore, the spatial lag distances of the noncontiguous elements from the main body of nursery proximity patterns provide an estimate of the approximate distance of spread of rain-splashed inoculum. Although these rain splash patterns of secondary foci have been visualized from isopath maps in previous work (12), distance estimates based on lag distances between discontinuous elements within individual proximity patterns, such as those from this study, have not been measured previously. Thus, SLA provides a means to estimate distance that inoculum is splash-disseminated by estimating the spatial distance (lags) between primary and secondary foci and the orientation of these secondary foci (discontinuous elements of the proximity pattern) in relation to the primary focus.

In contrast, the proximity patterns associated with the two

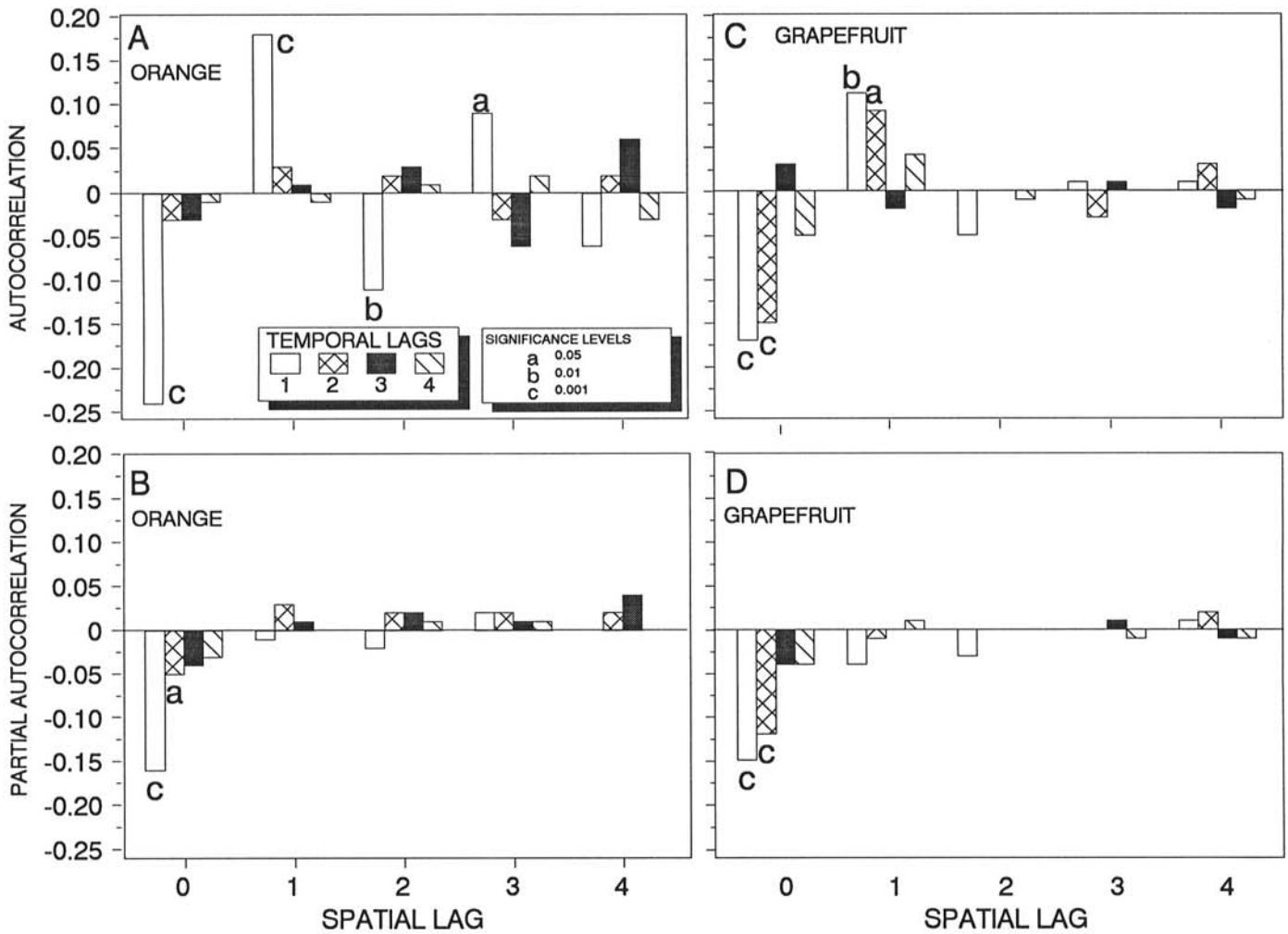

Fig. 7. Spatiotemporal autocorrelations and partial autocorrelations for **A** and **B,** orange grove plots, and **C** and **D,** grapefruit grove plots in central Argentina infested with citrus canker. Analysis was performed with the STAUTO program, with a square-proximity pattern and binary weighting. Logit(incidence) and simultaneous spatial and temporal differencing were used to assure spatial and temporal stationarity.

citrus grove plots generally lacked noncontiguous elements. Because of the greater spacing between individual trees in groves compared with that in nurseries, bacteria were splash-dispersed to the nearest neighboring tree downwind and rarely skipped trees. Thus, the proximity patterns associated with groves were more contiguous and elongated, as indicated by the greater association of diseased quadrats downwind (Fig. 2).

ST autocorrelation analysis. ST autocorrelation analysis illustrated the development of patterns over time but provided no information on the mechanisms that accounted for this development. On the other hand, the STARIMA model gave insight into the type of mechanisms responsible for pathogen spread and disease development, but the implications of STARIMA model structure were difficult to visualize (1). A STARIMA model was judged to be appropriate for all of the data because of the effectiveness of the spatial and temporal differencing in achieving stationarity and the appropriateness of a mixed model in each case.

Perhaps the most interesting aspect of our ST autocorrelation analyses was the high degree of similarity among STARIMA models for the three nursery data sets (Fig. 5, Tables 2 and 3), despite apparent differences in trends of the spatial autocorrelations and partial autocorrelations (Fig. 4). Our results indicate the existence of a common underlying process for citrus canker epidemics in the three nurseries that can be manifested in various temporal trends of spatial autocorrelation. This process is reflected in the close lattice structure of plants in citrus nurseries, which influences spread primarily by splash dissemination of bacteria to neighboring plants. This was the predominant trend throughout the epidemics. However, this trend was combined with coalescence of secondary foci predominantly during the last few assessment dates. Conversely, it is easy to overemphasize the significance of differences in temporal trends of spatial pattern, especially because the rapid increase in disease progress during the last few assessment dates for all three nurseries was related to single rainstorms combined with high winds.

In contrast to the ST autocorrelation analysis of nursery data, there were distinct differences in STARIMA model structure for the orange and grapefruit groves with respect to moving-average components (Fig. 7). In particular, the models for the orange and grapefruit groves included higher-order spatial and temporal moving-average terms, (4,1) and (1,2), respectively, than those for the nursery data. Higher-order spatial autocorrelations were also indicated by SLA analysis for the grapefruit grove compared with that for the orange grove. Disease increased more rapidly and spread more quickly because of the higher susceptibility of grapefruit than of orange to infection by *X. c. citri* (6,10,17). This higher level of disease, which occurred earlier in the epidemic in the grapefruit grove, may have contributed to higher-order spatial and temporal correlations for grapefruit.

The two analytical systems used in this study, SLA analysis and ST autocorrelation analysis, are complementary, but they differ significantly in their approach to spatial analysis. In SLA analysis, all quadrats or counts are compared with all others in the spatial matrix, whereas ST autocorrelation analysis compares all quadrats with surrounding quadrats located in predetermined proximity patterns (e.g., square, rook, queen, bishop, etc.) at increasing spatial lags. Thus, SLA analysis provides a more thorough means of visualizing the complexity of proximity patterns associated with plant disease epidemics at single points in time than ST autocorrelation analysis. The weakness of SLA analysis is the lack of a statistical means for comparison of these proximity patterns over time. This additional temporal comparison is the strength of ST autocorrelation analysis, which allows inferences to be drawn about spatial and temporal processes simultaneously. In this study, SLA analysis provided a clear picture of spatial proximity patterns and allowed us to examine the spatial processes that contributed to the development of these patterns (for example, splash dispersal and splash dispersal augmented by wind). ST autocorrelation analysis helped to confirm these spatial processes and accounted for the evolution of the spatial patterns over time (for example, the detection of the coalescence of primary and secondary foci). Consequently, we believe that the concurrent use of both analytical approaches led to a more thorough understanding of the spatial and temporal dynamics of citrus canker. In particular, the results from this study have confirmed previous conjectures concerning splash dispersal distances between primary and secondary foci and orientation of secondary foci in relation to the primary focus, and they provided new insight into the temporal stability and/or decay of spatial patterns of citrus canker in relationship to environmental processes.

LITERATURE CITED

1. Bennett, R. J. 1975. The representation and identification of spatio-temporal systems: An example of population diffusion in North-West England. Trans. Inst. Br. Geogr. 66:73-94.
2. Campbell, C. L., and Madden, L. V. 1990. Introduction to Plant Disease Epidemiology. John Wiley & Sons, Somerset, NJ.
3. Campbell, C. L., and Noe, J. P. 1985. The spatial analysis of soilborne pathogens and root diseases. Annu. Rev. Phytopathol. 23:129-148.
4. Cliff, A. D., and Ord, J. K. 1981. Spatial Processes: Models and Applications. Pion Ltd., London.
5. Danós, E., Berger, R. D., and Stall, R. E. 1984. Temporal and spatial spread of citrus canker within groves. Phytopathology 74:904-908.
6. Danós, E., Bonazzola, R., Berger, R. D., Stall, R. E., and Miller, J. W. 1984. Progress of citrus canker on some species and combinations in Argentina. Proc. Fla. State Hortic. Soc. 94:15-18.
7. Gottwald, T. R., Aubert, B., and Huang, Ke Long. 1990. Spatial pattern analysis of citrus greening in Shantou, China. Proc. Int. Conf. Citrus Virologists, 11th. 11:421-427.
8. Gottwald, T. R., and Graham, J. H. 1990. Spatial pattern analysis of epidemics of citrus bacterial spot in Florida citrus nurseries. Phytopathology 80:181-190.
9. Gottwald, T. R., Graham, J. H., and Egel, D. S. 1992. Analysis of foci of Asiatic citrus canker in a Florida citrus orchard. Plant Dis. 76:389-396.
10. Gottwald, T. R., McGuire, R. G., and Garran, S. 1988. Asiatic citrus canker: Spatial and temporal spread in simulated new planting situations in Argentina. Phytopathology 78:739-745.
11. Gottwald, T. R., Richie, S. M., and Campbell, C. L. 1992. LCOR2-Spatial correlation analysis software for the personal computer. Plant Dis. 76:213-215.
12. Gottwald, T. R., Timmer, L. W., and McGuire, R. G. 1989. Analysis of disease progress of citrus canker in nurseries in Argentina. Phytopathology 79:1276-1283.
13. Koizumi, M. 1981. Citrus canker. Pages 8-12 in: Citrus Diseases in Japan. T. Miyakawa and A. Yamaguchi, eds. Japan Plant Protection Association, Tokyo.
14. Koizumi, M. 1985. Citrus canker: The world situation. Pages 2-7 in: Citrus Canker: An International Perspective. L. W. Timmer, ed. University of Florida Institute of Food and Agricultural Science, Gainesville.
15. Madden, L. V., Reynolds, K. M., Pirone, T. P., and Raccah, B. 1988. Modeling of tobacco virus epidemics as spatio-temporal autoregressive moving-average processes. Phytopathology 78:1361-1366.
16. Modjeska, J. S., and Rawlings, J. O. 1983. Spatial correlation analysis of uniformity data. Biometrics 39:373-384.
17. Nicot, P. C., Rouse, D. I., and Yandell, B. S. 1984. Comparison of statistical methods for studying spatial patterns of soilborne plant pathogens in the field. Phytopathology 74:1399-1402.
18. Noe, J. P., and Campbell, C. L. 1985. Spatial pattern analysis of plant parasitic nematodes. J. Nematol. 17:86-93.
19. Reedy, B. C. 1984. Incidence of bacterial canker of citrus in relation to weather. Geobios New Rep. 3:39-41.
20. Reynolds, K. M., and Madden, L. V. 1988. Analysis of epidemics using spatio-temporal autocorrelation. Phytopathology 78:240-246.
21. Reynolds, K. M., Madden, L. V., and Ellis, M. A. 1988. Spatio-temporal analysis of epidemic development of leather rot of strawberry. Phytopathology 78:246-252.
22. Serizawa, S., and Inoue, K. 1975. Studies on citrus canker. III. The influence of wind blowing on infection. Bull. Schizuoka Pref. Citrus Exp. Stn. 11:54-67.
23. Serizawa, S., Inoue, K., and Goto, M. 1969. Studies on citrus canker. I. Dispersal of the citrus canker organism. Bull. Schizuoka Pref. Citrus Exp. Stn. 8:81-85.
24. Upton, G., and Fingleton, B. 1985. Spatial Pattern Analysis by Example. John Wiley & Sons, Chichester, England.